Trapping Low-mass Planets at the Inner Edge of the Protostellar Disk

Brasser, R.; Matsumura, S.; Muto, T.; Ida, S.

Published in:
Astrophysical Journal Letters

DOI:
10.3847/2041-8213/aada18

Publication date:
2018

Document Version
Publisher's PDF, also known as Version of record

The Astrophysical Journal Letters, 864:L8 (6pp), 2018 September 1 https://doi.org/10.3847/2041-8213/aada18

Trapping Low-mass Planets at the Inner Edge of the Protostellar Disk

R. Brasser[1], S. Matsumura[2], T. Muto[3], and S. Ida[1]
[1] Earth Life Science Institute, Tokyo Institute of Technology, Tokyo, Japan
[2] Division of Physics, University of Dundee, Dundee, UK
[3] Division of Liberal Arts, Kogakuin University, Tokyo, Japan
Received 2018 July 18; revised 2018 August 10; accepted 2018 August 12; published 2018 August 29

Abstract

The formation of multiple close-in low-mass exoplanets is still a mystery. The challenge is to build a system wherein the outermost planet is beyond 0.2 au from the star. Here, we investigate how the prescription for type I planet migration affects the ability to trap multiple planets in a resonant chain near the inner edge of the protostellar disk. A sharp edge modeled as a hyperbolic tangent function coupled with supersonic corrections to the classical type I migration torques results in the innermost planets being pushed inside the cavity through resonant interaction with farther planets because migration is starward at slightly supersonic eccentricities. Planets below a few Earth masses are generally trapped in a resonant chain with the outermost planet near the disk edge, but long-term stability is not guaranteed. For more massive planets the migration is so fast that the eccentricity of the innermost resonant pair is excited to highly supersonic levels due to decreased damping on the innermost planet as it is pushed inside the cavity; collisions frequently occur, and the system consists of one or two intermediate-mass planets residing closer to the star than the disk's inner edge. We found a neat pileup of resonant planets outside the disk edge only if the corotation torque does not rapidly diminish at high eccentricity. We call for detailed studies on planet migration near the disk's inner edge, which is still uncertain, and for an improved understanding of eccentricity damping and disk torques in the supersonic regime.

Key words: celestial mechanics – planets and satellites: dynamical evolution and stability – planets and satellites: formation

1. Introduction

Preventing low-mass planets from migrating to their host star is a long-standing problem. Mergers with their host star can be prevented if the protostellar disk has a sharp inner edge at a few stellar radii (Masset et al. 2006; Ogihara et al. 2010). Terquem & Papaloizou (2007) showed that migrating protoplanets usually end up in resonances. Some of these resided inside the disk's inner cavity. Ogihara & Ida (2009) also build a resonant chain of low-mass protoplanets that stalled near the disk's inner edge when the migration was artificially slowed down and the reduction of the corotation torque was ignored. Recently, Izidoro et al. (2017) trapped a high number of low-mass planets outside the disk edge in a resonant chain that subsequently needed to break to account for the currently observed exoplanet period distribution. On the other hand, Matsumura et al. (2017) had trouble trapping multiple planets near the disk's inner edge, even though their migration prescription was very similar to that of Izidoro et al. (2017): both include supersonic corrections to the migration and eccentricity damping timescales. Terquem & Papaloizou (2007) also included such corrections, but they followed the prescription of Papaloizou & Larwood (2000), while Izidoro et al. (2017) and Matsumura et al. (2017) followed Coleman & Nelson (2014). The simulations of Matsumura et al. (2017) usually resulted in one or two hot Neptune planets rather than a multiplet of smaller planets. The disparity between all of these results warrants further study.

2. Disk Model and Planet Migration

We employ the disk model of Ida et al. (2016), which is based on Garaud & Lin (2007) and Oka et al. (2011). Here, we briefly summarize their model.

2.1. Disk Parameters

We assume steady-state accretion onto the Sun. The gas accretion rate is

$$\dot{M}_* = 3\pi\alpha\Sigma H^2\Omega_{\rm K}, \tag{1}$$

where Σ is the gas surface density, H is the disk scale height, and $\Omega_{\rm K}$ is the orbital frequency. The α-viscosity is assumed to be constant (Shakura & Sunyaev 1973). The disk scale height is $H = c_s/\Omega_{\rm K}$, where $c_s = (\gamma k_B T/\mu m_{\rm prot})^{1/2}$ with $\gamma = 7/5$, k_B is the Boltzmann constant, $m_{\rm prot}$ the proton mass, and $\mu = 2.3$ is the mean atomic mass of the gas. Now $\dot{M}_*$ evolves as (Hartmann et al. 1998)

$$\log\left(\frac{\dot{M}_*}{M_\odot\ {\rm yr}^{-1}}\right) = -8 - \frac{7}{5}\log\left(\frac{t}{1\ {\rm Myr}} + 0.1\right). \tag{2}$$

The extra 0.1 Myr avoids the logarithmic singularity (Bitsch et al. 2015).

For solar-type stars, the midplane temperature in the viscous part of the disk is

$$T = 200\alpha_3^{-1/5}\dot{M}_{*8}^{2/5}\left(\frac{r}{1\ {\rm au}}\right)^{-9/10}, \tag{3}$$

where r is the distance to the star and we defined $\dot{M}_{*8} = \dot{M}_*/10^{-8}\,M_\odot\ {\rm yr}^{-1}$ and $\alpha_3 = \alpha/10^{-3}$. The reduced scale height $h = H/r$ is

$$h = 0.034\alpha_3^{-1/10}\dot{M}_{*8}^{1/5}\left(\frac{r}{1\ {\rm au}}\right)^{1/20}. \tag{4}$$

Equations (1), (3), and (4) may be combined to compute the surface density of the gas.

2.2. Disk Inner Edge Implementation

Near the star, the surface density of the disk is assumed to smoothly decrease to zero. Cossou et al. (2014) suggested that

$$\Sigma = \Sigma(r_{\rm tr})\tanh\left(\frac{r - r_{\rm in}}{H}\right), \quad (5)$$

where $r_{\rm tr}$ is the planet trap location from the star; here, the surface density is maximal. The trap is at $r_{\rm tr} = 0.1$ au for solar-type stars; it is unclear how reliable the employed disk model is closer to the star where MHD effects become important. Trapping planets requires a sharp edge (Masset et al. 2006; Ogihara et al. 2010). Therefore, we set the inner edge of the disk at $r_{\rm in} = 0.95r_{\rm tr}$, which is approximately 2 scale heights inside of $r_{\rm tr}$. The surface density slope is computed as

$$s \equiv -\frac{d\ln\Sigma}{d\ln r} = -\frac{1}{h}\left(\frac{1}{x} - x\right). \quad (6)$$

where $x = \tanh\left[\frac{(r - r_{\rm in})}{H}\right]$. Now, $s \to -\infty$ as $r \to r_{\rm in}$ and all planets in the type I regime cease migrating at or near $r_{\rm tr}$.

To avoid the divergence of s at $r_{\rm in}$, which could possibly cause numerical artifacts, we also tested a linear decrease in Σ, for which $s = -1$. The resulting discontinuity of s at $r_{\rm tr}$ was made smooth via a linear connection over the length $0.2H$.

2.3. Planet Migration

The gas disk exerts torques and tidal forces on the embedded planets that result in a combined effect of radial migration and the damping of the eccentricity and inclination. For low-mass planets the migration is of type I (Tanaka et al. 2002), while massive planets that are able to clear the gas in their vicinity experience type II migration (Lin & Papaloizou 1986). Here, we are only interested in the former.

We follow Coleman & Nelson (2014) for computing the torque and the direction of migration. Their formulae are based on Paardekooper et al. (2011) for the torque and on Fendyke & Nelson (2014) and Cresswell & Nelson (2008) for the eccentricity damping, including corrections to the damping timescale and corotation torque in the supersonic regime when the eccentricity $e > h$. We restrict ourselves to planar orbits. The normalized torque is (Paardekooper et al. 2011)

$$\frac{\gamma\Gamma}{\Gamma_0} = \frac{\Gamma_{\rm C}}{\Gamma_0}F_{\rm C} + \frac{\Gamma_{\rm L}}{\Gamma_0}F_{\rm L} \quad (7)$$

where $\Gamma_{\rm C} = \Gamma_{\rm C,baro} + \Gamma_{\rm C,ent}$ and $\Gamma_{\rm L}$ are the corotation and Lindblad torques, respectively, and $\Gamma_0 = (m_p/m_\odot)^2(H/r)^{-2}\Sigma\Omega_{\rm K}^2$ is a normalization constant. The corotation torque in a non-isothermal disk with thermal diffusion becomes

$$\begin{aligned}\Gamma_{\rm C,baro} &= F(p_\nu)G(p_\nu)\Gamma_{\rm hs,baro} \\ &\quad + [1 - K(p_\nu)]\Gamma_{\rm C,lin,baro}, \\ \Gamma_{\rm C,ent} &= F(p_\nu)F(p_\chi)[G(p_\nu)G(p_\chi)]^{1/2}\Gamma_{\rm hs,ent} \\ &\quad + \{[1 - K(p_\nu)][1 - K(p_\chi)]\}^{1/2}\Gamma_{\rm C,lin,ent}. \end{aligned} \quad (8)$$

Here, p_ν and p_χ depend on m_p, h, and α (Paardekooper et al. 2011). The functions $F(p)$, $G(p)$, and $K(p)$ determine the amount of torque saturation and are dependent on the planet mass and disk scale height (Paardekooper et al. 2011). In steady state, $q + s = \frac{3}{2}$, where $q = -\frac{d\ln T}{d\ln r}$. The remaining contributions are then (Paardekooper et al. 2011)

$$\begin{aligned}\frac{\gamma\Gamma_{\rm L}}{\Gamma_0} &= -2.5 - 1.7q + 0.1s = -2.35 - 1.8q \\ \frac{\gamma\Gamma_{\rm hs,baro}}{\Gamma_0} &= 1.1(3/2 - s) = 1.1q \\ \frac{\gamma\Gamma_{\rm C,lin,baro}}{\Gamma_0} &= 0.7(3/2 - s) = 0.7q \\ \frac{\gamma\Gamma_{\rm hs,ent}}{\Gamma_0} &= \frac{7.9\xi}{\gamma} = 5.6\left(\frac{7}{5}q - \frac{3}{5}\right) \\ \frac{\gamma\Gamma_{\rm C,lin,ent}}{\Gamma_0} &= \left(2.2 - \frac{1.4}{\gamma}\right)\xi = 0.8\left(\frac{7}{5}q - \frac{3}{5}\right), \end{aligned} \quad (9)$$

where $\xi = -\frac{d\ln S}{d\ln r} = q - (\gamma - 1)s = \frac{7}{5}q - \frac{3}{5}$ is the negative entropy gradient. The F, G, and K functions disallow writing the explicit dependence of Γ on q, but generally $\Gamma_{\rm C} \propto q$ and $\Gamma_{\rm L} \propto -q$.

The factors $F_{\rm L}$ and $F_{\rm C}$ are

$$\begin{aligned}\ln F_{\rm C} &= -\frac{e}{e_{\rm f}}, \\ F_{\rm L} &= \frac{1 + (0.444\hat{e})^{1/2} + (0.352\hat{e})^6}{1 - (0.495\hat{e})^4}, \end{aligned} \quad (10)$$

where $e_{\rm f} = 0.01 + \frac{1}{2}h$ and $\hat{e} = e/h$. The eccentricity damping timescale $\tau_e = -e/\dot{e}$ is (Cresswell & Nelson 2008)

$$\tau_e = 1.282t_{\rm wav}(1 - 0.14\hat{e}^2 + 0.06\hat{e}^3), \quad (11)$$

where the wave timescale is (Tanaka & Ward 2004)

$$t_{\rm wav} = \left(\frac{M_*}{m_p}\right)\left(\frac{M_*}{\Sigma r^2}\right)h^4\Omega_K^{-1}. \quad (12)$$

The "migration timescale" (Cresswell & Nelson 2008) is

$$\tau_m = -\frac{t_{\rm wav}\Gamma_0}{h^2\Gamma}. \quad (13)$$

Despite its name, τ_m is *not* the actual migration timescale. By definition, $\tau_m = -L/\dot{L}$ (Cresswell et al. 2007) and $L = m_p\sqrt{GM_\odot a(1 - e^2)}$ so that $\tau_m \approx 2\tau_a$ when $e \approx 0$. Here, $\tau_a = -a/\dot{a}$ is the timescale for semimajor axis evolution. In the supersonic regime, hydrodynamical simulations show that the torque reverses direction when $e \sim 2h$ and the torque is maximal (and positive) when $e \sim 4h$ (Cresswell & Nelson 2008). However, Cresswell & Nelson (2008) show that the planet always migrates inward, despite the torque reversal at high eccentricity. The analytical approach of Muto et al. (2011) agrees with this result: inward migration persists at high eccentricity. Therefore, it is incorrect to use τ_m to compute the evolution of the semimajor axis; τ_a should be used instead (Matsumura et al. 2017). This is

$$\tau_a^{-1} = 2\tau_m^{-1} + \frac{2e^2}{(1 - e^2)}\tau_e^{-1}. \quad (14)$$

Izidoro et al. (2017) adopted τ_m for the migration timescale, which led to the aforementioned difference. All timescales are

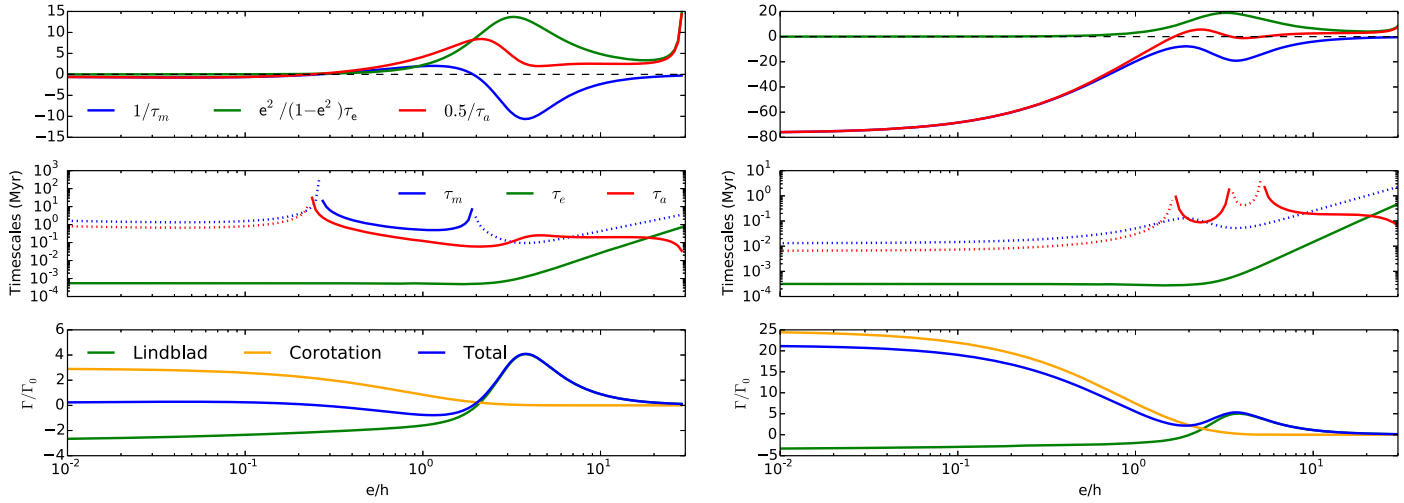

Figure 1. Plot of various timescales and normalized torques vs. eccentricity for a 1 $M_\oplus$ planet. Left: at 1 au. Right: at 0.099 au. Dotted lines are for negative values.

positive for inward migration and negative for outward migration.

2.4. Planet Migration Near the Disk Edge

The reciprocal migration timescale, $0.5\tau_a^{-1}$, and its two components, τ_m^{-1} and $e^2(1-e^2)^{-1}\tau_e^{-1}$, are plotted in the top panels of Figure 1 for the fiducial case (all supersonic corrections enabled) as a function of planetary eccentricity. The middle panels show the individual timescales, and the bottom panels depict the normalized torques. The left column pertains to a 1 $M_\oplus$ planet at 1 au, while to the right the planet is at 0.099 au. The outcome for the linear edge prescription is very similar.

At 1 au when $e \ll h$, we generally have $\tau_e \ll \tau_a \sim \tau_m$, and angular momentum transfer between the disk and the planet usually leads to *inward* migration ($\tau_a > 0$). The example in Figure 1, however, has outward migration when $e \lesssim 0.2h$ because for this mass and α the strength of the corotation torque slightly exceeds that of the Lindblad torque (Paardekooper et al. 2011; Brasser et al. 2017); see the bottom panels of Figure 1. When $e \gg h$, we have $\tau_e \sim 2e^2(1-e^2)^{-1}\tau_a \ll |\tau_m|$, and the *inward* migration is the result of eccentricity damping at constant angular momentum. These two cases are common to all the combinations of the torque formulae. However, the relations for τ_e, τ_a, and τ_m are different when $e \sim h$ for the various configurations.

At 0.099 au (near the disk's inner edge), these two cases are also applicable, except that the difference between τ_e and τ_a when $e \ll h$ is smaller than at 1 au. When $e \sim h$ at 0.099 au, however, the relations for τ_e, τ_a, and τ_m are different from that at 1 au.

These fundamental differences are clearly seen between the two panels, assuming that Equation (7) and the supersonic corrections are applicable at the disk edge.

Suppose there is a single planet at $r_{\rm tr}$. When a second planet approaches the first one, it is likely to become trapped in resonance (Petrovich et al. 2013). The equilibrium eccentricity of both planets is the result of the balance of migration and damping and is $e_{\rm eq} \approx 1.3h$ (Goldreich & Schlichting 2014). At this eccentricity, $\tau_m < 0$, but $\tau_a > 0$ when $r_{\rm in} < r < r_{\rm tr}$, and the planets migrate *inward*. The innermost planet has its eccentricity excited as the outer planet pushes the pair starward until the latter reaches $r_{\rm tr}$; the inner planet is now parked inside the disk cavity. Should a third, fourth, and additional planets approach the inner pair, the mechanism will likely repeat itself until the outermost planet is at the disk edge and all the other planets are inside of it, or until the outermost planets can no longer push the inner chain deeper into the cavity due to the chain's inertia.

The above arguments assume that the planet is surrounded by a gas disk on both sides. Near the edge, the torque is one-sided: at the inner disk edge there is only the outer Lindblad torque that pushes the planet inward, but no inner Lindblad torque. Liu et al. (2017) implemented simplified one-sided corotation, and Lindblad torques and showed that small planets could be trapped near the edge, but their implementation only works for an infinitely sharp edge.

3. Numerical Methods

To study the behavior of planets near the disk edge, we performed a set of numerical *N*-body simulations consisting of a solar-mass star and four equal-mass planets. These integrations used the symplectic *N*-body code SyMBA (Duncan et al. 1998), which was heavily modified to include the effects of eccentricity and inclination damping as well as planet migration by the gas disk according to the formulation above (Matsumura et al. 2017).

We initially place the planets beyond their 2:1 mean-motion resonances. The planet's masses are all either 0.1, 0.5, 2, 3, 5, or 8 Earth masses ($M_\oplus$). We compute the torques at each time step for each body; we apply eccentricity damping only when $e > 0.001h$. There is a surface density maximum at $r_{\rm tr} = 0.1$ au from the star. Closer to the star than the disk edge at $r_{\rm in}$ there is no migration nor damping.

Simulations are run for 2 Myr with a time step of 0.146 days. Bodies are removed when they are closer than 0.02 au or farther than 100 au from the star, or when they collide. We assume perfect accretion during collisions. Initially, $\dot{M}_{*8} = 1$ and $\alpha_3 = 1$. For simplicity, we keep α fixed despite its potential to change close to the star where MRI effects (Bai & Stone 2013) and disk ionization are important (Gammie 1996). The value of α affects the torque in a complicated manner as described in Equation (8) (Paardekooper et al. 2011; Brasser et al. 2017). As we show below, the most important factor in altering the torque is the

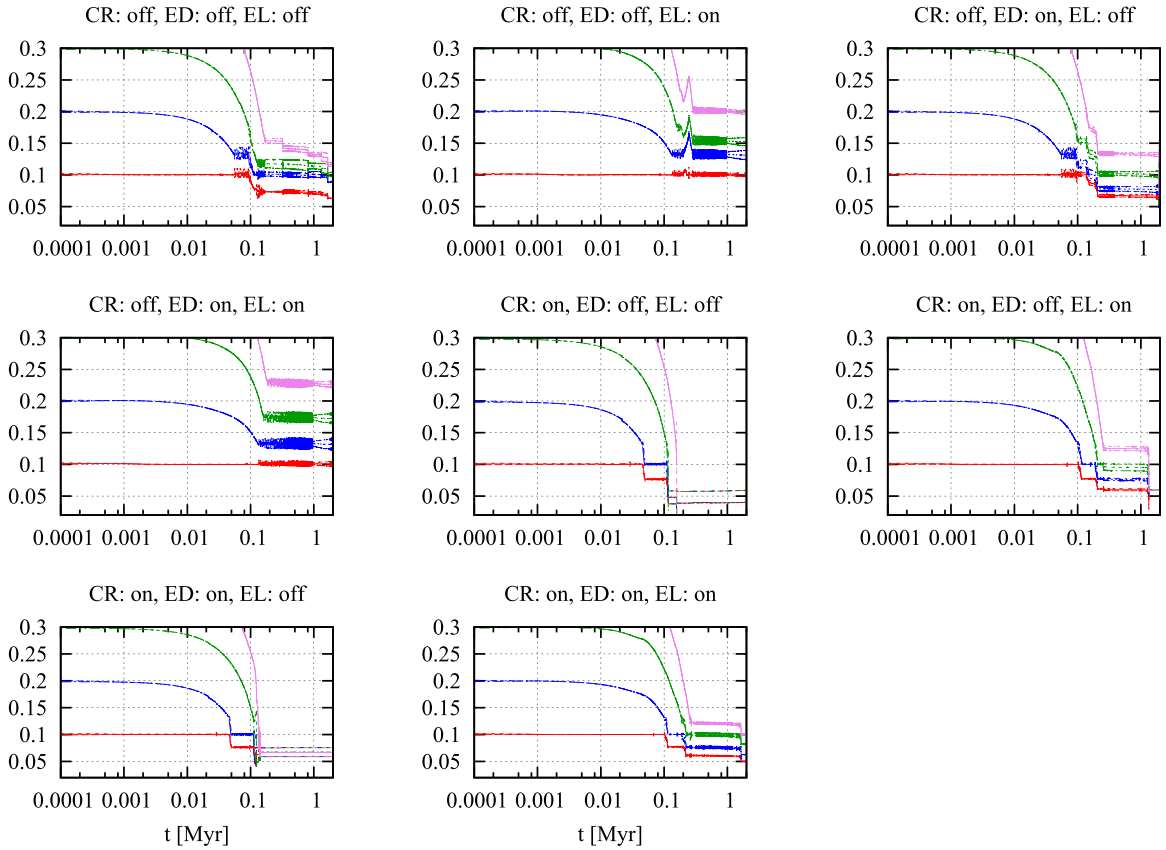

Figure 2. Migration of four 2 $M_\oplus$ planets toward the disk edge. The panels all depict different migration prescriptions.

supersonic corrections, in particular, the corotation reduction, F_C, which is independent of $\dot{M}_*$ and α.

We test the dependence of the migration on eccentricity by selectively enabling or disabling the supersonic corrections to the corotation torque, the Lindblad torque, and the eccentricity damping timescale. Apart from Masset et al. (2006), we are not aware of any systemic hydrodynamical studies of embedded planets near the disk edge. Motivated by this, we enable or disable ("on" or "off") the corotation reduction term (F_C in Equation (10), "CR") as well as the supersonic corrections to the eccentricity damping timescale (the term inside the parentheses in Equation (11), "ED") and to the Lindblad torque (F_L in Equation (10), "EL"). This simple approach should suffice in the absence of more detailed torque prescriptions near the edge.

4. Results

We show an example of the evolution of four planets of 2 $M_\oplus$ near the disk edge in Figure 2. The evolution is very different depending on the migration prescription. In the broadest sense, the planets become trapped in resonances outside the disk edge when the corotation reduction F_C is *not* applied, and preferably when the supersonic correction to the Lindblad torque, F_L, *is* applied. If either or both of these are applied, multiple planets will end up inside the disk cavity.

This outcome is in contrast with Izidoro et al. (2017) because they use τ_m to compute the semimajor axis evolution of the planets instead of τ_a. Since $\tau_m < 0$ at the disk edge for any value of e, their innermost planet can often stall any additional incoming planets even if it or the others are supersonic, though the exact evolution is mass dependent. For example, in their Figure 4, the innermost planet is 10 $M_\oplus$ and all planets are trapped beyond 0.1 au, while in their Figure 5, the innermost planet (initially) has a few $M_\oplus$ and a chain of planets is pushed inward as more massive planets migrate in. In resonance, the approximation $\tau_a = \tau_m$ breaks down because the planets are supersonic; Equation (14) should be used instead.

Our results are also in disagreement with Ogihara et al. (2010), who found that a sharp edge was able to prevent the planets from falling into the cavity. Ogihara et al. (2010) concluded that the imbalance of increased drag on the planet at aphelion versus little to no drag at perihelion caused the planet to be stationary at the edge with a non-zero eccentricity. However, they did not include any supersonic corrections to their migration formulae.

In our approach, the edge is fairly sharp, but the tanh function quickly flattens beyond $\tanh 1 \approx 0.76$. Thus, if the planet is near r_{tr}, the drag at aphelion and perihelion is within 25% if the eccentricity is $e \sim h$. Only when the planet is roughly halfway between r_{in} and r_{tr} is the drag at aphelion (where the tanh function is $\sim$1) much stronger than at perihelion (where it is $\sim$0) and do we possibly recover the situation from Ogihara et al. (2010), but only if the supersonic reduction of the corotation torque is ignored.

4.1. Different Torque Prescriptions Yield Different Outcomes

What aspects of the torque prescription are responsible for the different behaviors at the edge? At low eccentricity, outward migration is caused by the corotation torque while inward migration is caused by the Lindblad torque; the latter only depends on the temperature and surface density gradients (Paardekooper et al. 2011). When supersonic corrections are

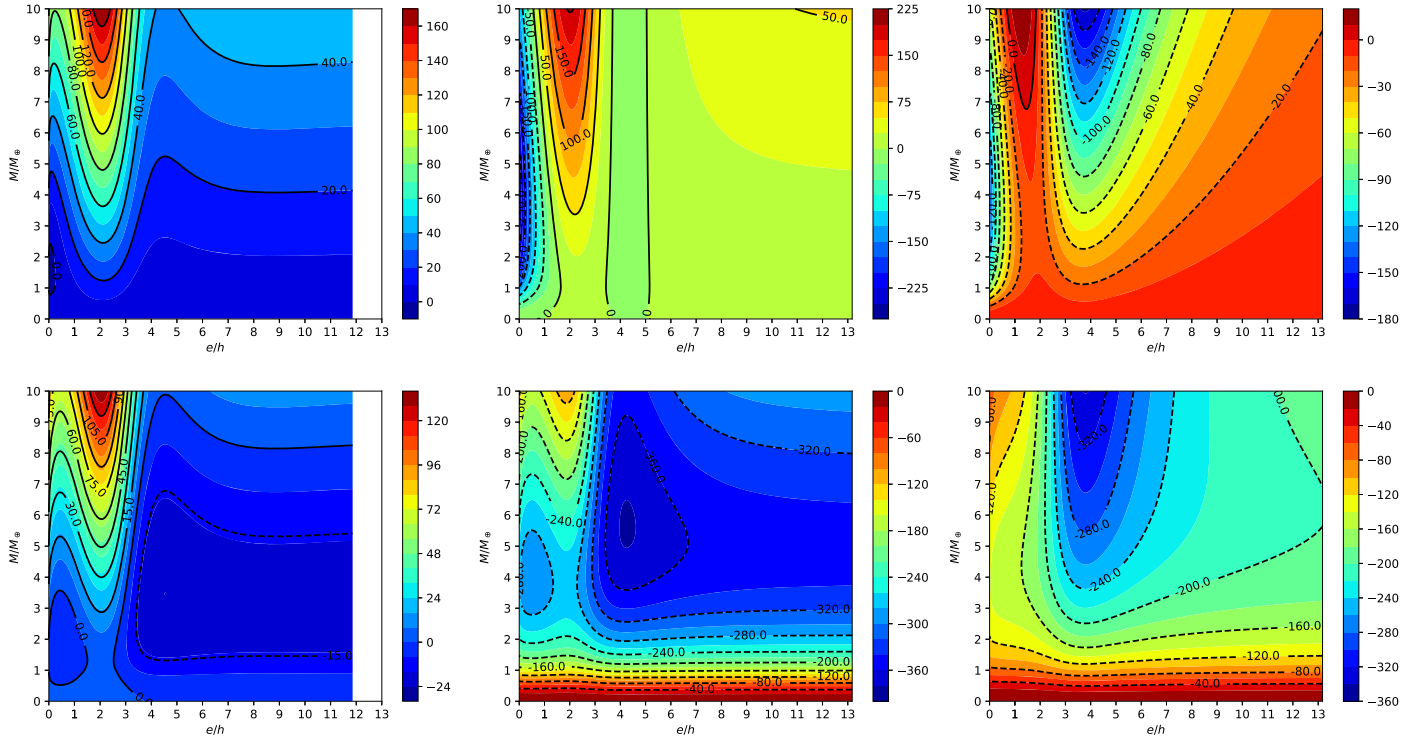

Figure 3. Left: contour map of τ_a^{-1} in Myr^{-1} for a planet of 1 $M_\oplus$ at 1 au as a function of e/h and m_p. Middle: same as the left panel, but at 0.099 au. Right: τ_m^{-1} in Myr^{-1} at 0.099 au. Bottom panels are the same as the top panels, but now $F_C = 1$, i.e., there is no corotation reduction at high eccentricity.

considered, the total torque also depends on e. In general, with our prescription, τ_a^{-1} is not a monotonically decreasing function of e, but instead has a peak near $e \sim h$ and a trough at $e \sim 4h$ (Cresswell & Nelson 2008). This behavior is caused by how τ_m varies with eccentricity, and also because the maxima of τ_m^{-1} and $e^2/(1-e^2)\tau_e^{-1}$ do not coincide (top right panel of Figure 1). The migration rate peaks for all planetary masses near $e \sim 0.5h$ reach a minimum when $e \sim 2h$ and a further maximum when $e \sim 4.5h$. This non-monotonic behavior is inconsistent with the analytical results of Muto et al. (2011).

However, the behavior is different when the planet is inside of the trap. At very low eccentricity, and for nearly all planet masses, τ_a^{-1} is negative and low, implying slow outward migration. Migration is inward when $e \sim h$ and outward again at higher eccentricity. The top row of Figure 3 is a contour map showing τ_a^{-1} at 1 au (left), near the disk's inner edge (middle), together with τ_m^{-1} near the edge (right).

The region of inward migration near moderate e prevents the trap from stalling migrating planets in resonances, and any planet situated at $r_{\rm tr}$ is pushed deep inside the cavity, together with any planets interior to it. Therefore, the outcome of numerical simulations and the ability to trap planets near the disk edge depends on the exact migration prescription employed. When using τ_m the migration is always outward.

Figure 2 suggests that eliminating the corotation reduction, F_C, and weakening the Lindblad torque by applying F_L provides the best prescription to trap multiple planets in resonance outside of $r_{\rm tr}$, assuming the current torque formulae hold near the edge (cf. Liu et al. 2017). The bottom row of Figure 3 shows similar contour maps, but now $F_C = 1$, i.e., there is no corotation reduction. The behavior is qualitatively different everywhere: at the edge, migration is always outward, but the strength is a complicated function of both the planetary mass and the eccentricity.

Hydrodynamical simulations show that the corotation torque weakens as the eccentricity increases and mostly disappears at $e \gtrsim 3h$ (Cresswell et al. 2007). It thus appears to be unphysical to remove the corotation reduction far from the disk edge, but it is unclear if this removal is applicable near the edge. The exponential reduction of Fendyke & Nelson (2014) does not appear to hold for low values of $h \lesssim 0.05$; the corotation reduction also depends on how the torque is measured. Their Figures 4 and 9 clearly show torque maxima near $e \sim 2.5h$ so that the exponential reduction may not be universally applicable. Clearly more work is needed, both on the reduction itself but also how it behaves near the disk edge.

In Figure 2, the bottom middle panel with all of the supersonic effects enabled was able to temporarily trap the planets in a resonance even though the innermost planets were pushed into the cavity. Increasing the corotation torque kept the planets outside of the cavity (CR: OFF). This structure does not hold for higher-mass planets because they migrate faster, and therefore excite themselves to higher eccentricities once the innermost planet is in the cavity and eccentricity damping is weak or nonexistent. An example is shown in Figure 4, which is the same as Figure 2, but now the planets are 5 $M_\oplus$.

5. Conclusions

The ability to trap multiple low-mass planets in a resonant chain outside the inner edge of the protostellar disk has been investigated. These low-mass planets execute type I migration that pulls them invariably toward the star. In the absence of a barrier, these would all collide with the star. The disk's inner edge could provide a trapping mechanism (Masset et al. 2006). We have tested two types of sharp inner edges of the disk: a hyperbolic tangent and a linear function, along with different migration prescriptions.

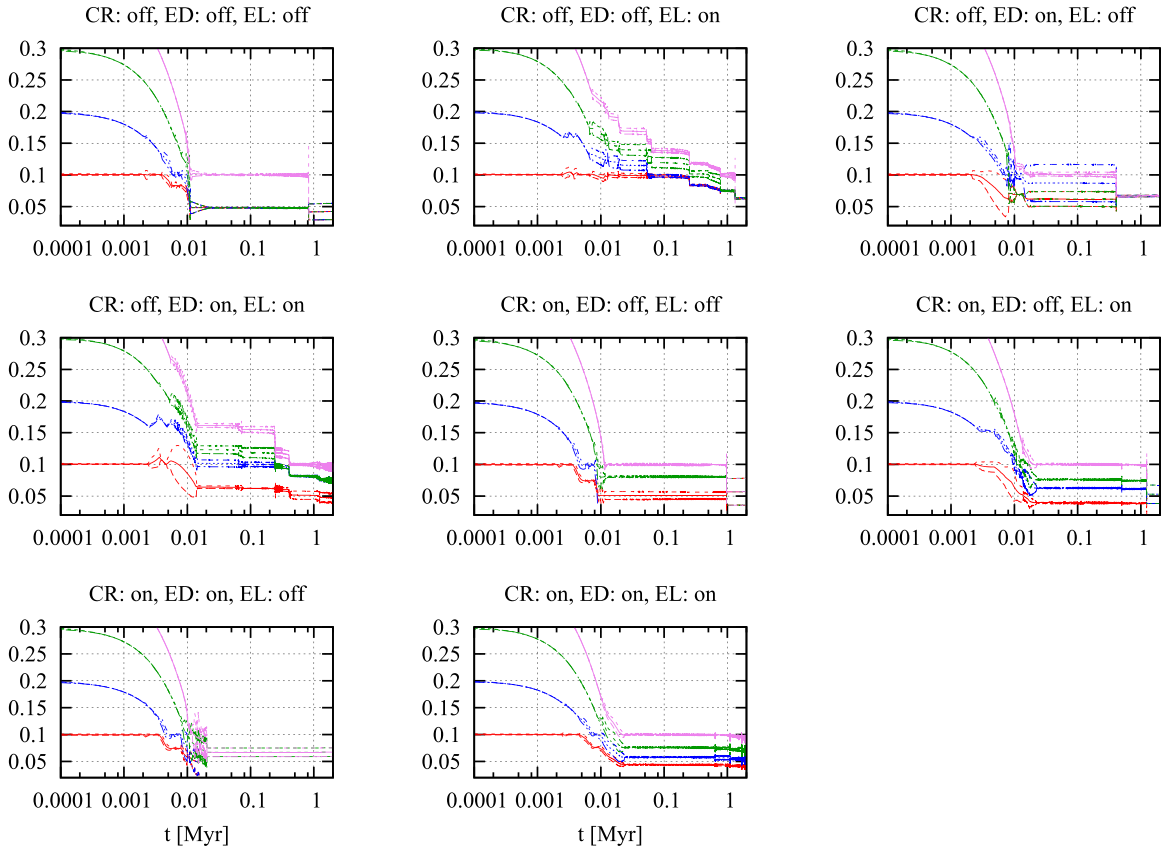

Figure 4. Same as Figure 2, but the planets are now 5 $M_\oplus$.

We find that a neat pileup of resonant planets outside the disk edge is established if the corotation torque does not rapidly diminish at high eccentricity. The expectation is that if the resonant chain of the planets remains outside the inner disk edge they eventually start orbit crossing and instigate a phase of giant impacts. This may account for formation of similar-sized, regularly spaced, non-resonant low-mass planets that are found to be common in relatively close-in regions by *Kepler* observations. However, the eccentricity damping and disk torques in the supersonic regime remain uncertain near the disk's inner edge. Due to resonant interactions, eccentricity is generally excited to values $e \sim h$ for which the migration is generally inward. Therefore, we call for detailed studies on eccentricity damping and disk torques in the supersonic regime and near the disk edge. Such studies will play an important role in understanding the common architecture of compact systems.

Note added in proof. We thank Ryan Miranda for pointing out that wave reflection at the disk edge could halt planet migration (Miranda & Dong 2018).

References

Bai, X.-N., & Stone, J. M. 2013, ApJ, 767, 30
Bitsch, B., Lambrechts, M., & Johansen, A. 2015, A&A, 582, A112
Brasser, R., Bitsch, B., & Matsumura, S. 2017, AJ, 153, 222
Coleman, G. A. L., & Nelson, R. P. 2014, MNRAS, 445, 479
Cossou, C., Raymond, S. N., Hersant, F., & Pierens, A. 2014, A&A, 569, A56
Cresswell, P., Dirksen, G., Kley, W., & Nelson, R. P. 2007, A&A, 473, 329
Cresswell, P., & Nelson, R. P. 2008, A&A, 482, 677
Duncan, M. J., Levison, H. F., & Lee, M. H. 1998, AJ, 116, 2067
Fendyke, S. M., & Nelson, R. P. 2014, MNRAS, 437, 96
Gammie, C. F. 1996, ApJ, 457, 355
Garaud, P., & Lin, D. N. C. 2007, ApJ, 654, 606
Goldreich, P., & Schlichting, H. E. 2014, AJ, 147, 32
Hartmann, L., Calvet, N., Gullbring, E., & D'Alessio, P. 1998, ApJ, 495, 385
Ida, S., Morbidelli, A., & Guillot, T. 2016, A&A, 591, A72
Izidoro, A., Ogihara, M., Raymond, S. N., et al. 2017, MNRAS, 470, 1750
Lin, D. N. C., & Papaloizou, J. 1986, ApJ, 309, 846
Liu, B., Ormel, C. W., & Lin, D. N. C. 2017, A&A, 601, A15
Masset, F. S., Morbidelli, A., Crida, A., & Ferreira, J. 2006, ApJ, 642, 478
Matsumura, S., Brasser, R., & Ida, S. 2017, A&A, 607, A67
Miranda, R., & Dong, L. 2018, MNRAS, 473, 5276
Muto, T., Takeuchi, T., & Ida, S. 2011, ApJ, 737, 37
Ogihara, M., Duncan, M. J., & Ida, S. 2010, ApJ, 721, 1184
Ogihara, M., & Ida, S. 2009, ApJ, 699, 824
Oka, A., Nakamoto, T., & Ida, S. 2011, ApJ, 738, 141
Paardekooper, S.-J., Baruteau, C., & Kley, W. 2011, MNRAS, 410, 293
Papaloizou, J. C. B., & Larwood, J. D. 2000, MNRAS, 315, 823
Petrovich, C., Malhotra, R., & Tremaine, S. 2013, ApJ, 770, 24
Shakura, N. I., & Sunyaev, R. A. 1973, A&A, 24, 337
Tanaka, H., Takeuchi, T., & Ward, W. R. 2002, ApJ, 565, 1257
Tanaka, H., & Ward, W. R. 2004, ApJ, 602, 388
Terquem, C., & Papaloizou, J. C. B. 2007, ApJ, 654, 1110